Dynamic phosphorylation of Hcm1 promotes fitness in chronic stress

Michelle M. Conti[1], Jillian P. Bail[1], Aurelia R. Reynolds[1], Linnea G. Budge[1], Mackenzie J. Flynn[1], Rui Li[1], Lihua Julie Zhu[1,2,3], Jennifer A. Benanti[1,*]

[1]Department of Molecular, Cell and Cancer Biology, University of Massachusetts Chan Medical School, Worcester, MA 01605.

[2]Department of Genomics and Computational Biology, University of Massachusetts Chan Medical School, Worcester MA 01605.

[3]Program in Molecular Medicine, University of Massachusetts Chan Medical School, Worcester MA 01605.

*Correspondence: jennifer.benanti@umassmed.edu

Abstract

Cell survival depends upon the ability to adapt to changing environments. Environmental stressors trigger an acute stress response program that rewires cell physiology, downregulates proliferation genes and pauses the cell cycle until the cell adapts. After the acute response is resolved, cells resume cycling but at a reduced rate. The importance of cell cycle changes for survival in chronic stress is not clear. Here, we show that dynamic phosphorylation of the yeast cell cycle-regulatory transcription factor Hcm1 is required to maintain fitness in chronic stress. Hcm1 is activated by cyclin dependent kinase (CDK) during S-phase and is inactivated by the phosphatase calcineurin (CN) in response to stressors that signal through increases in cytosolic Ca^{2+}. Expression of a constitutively active, phosphomimetic Hcm1 mutant reduces fitness in stress, suggesting Hcm1 inactivation is required for survival. However, a comprehensive analysis of Hcm1 phosphomutants revealed that Hcm1 activity is also important to survive stress, and that all mutants with fixed phosphorylation states are less fit in stress. Moreover, pulses of Hcm1 activity are necessary to maximize target gene expression in stress. These findings demonstrate that the expression levels of Hcm1 target genes influence fitness in stress and suggest that the dynamic phosphorylation of cell cycle regulators plays a crucial role in promoting survival in stressful environments.

Introduction

Cells are continuously exposed to stressors in the environment and must adapt to these challenges to survive and proliferate. Adaptation not only protects healthy cells from death, but conversely, it can promote the development of disease. For instance, cancer cells must adapt to stressful environments when they metastasize to distant sites [1,2], and fungal pathogens rely upon stress response pathways for survival within the host [3]. Despite the importance of this

25 process, the long-term changes that cells must undergo to maintain fitness and proliferation when
26 faced with chronic stress are poorly understood.

27 The acute stress response, which occurs immediately following exposure to an
28 environmental stressor, is conserved from yeast to humans and includes a downregulation of
29 protein synthesis and an upregulation of stress response genes [4,5]. In addition to these changes
30 that impact cell physiology, cell cycle-regulatory genes are downregulated, and cells undergo a
31 transient cell cycle arrest [6,7]. After cells adapt to the new environment, the acute stress
32 response is resolved and cells resume proliferation in the new environment, albeit at a reduced
33 rate [8–10]. Transient cell cycle arrest during the acute stress response is thought to be crucial to
34 promote long-term survival [9–11]. However, the importance of cell cycle changes for survival in
35 chronic stress is not well understood.

36 Some stressors signal through an increase in cytosolic Ca^{2+} and coordinate the stress
37 response program and cell cycle changes by activating the conserved Ca^{2+}-activated
38 phosphatase calcineurin (CN) [12,13]. CN activation leads to a decrease in expression of cell
39 cycle-regulatory genes and controls the length of cell cycle arrest, in combination with the stress-
40 activated MAPK Hog1/p38 [14]. One direct target of CN in budding yeast is the S-phase
41 transcription factor (TF) Hcm1 [15]. Hcm1 is a forkhead family transcriptional activator which, like
42 it's human homolog FoxM1, plays a crucial role in maintaining genome stability [16,17]. Hcm1
43 controls expression of key cell cycle genes including histone genes, downstream cell cycle-
44 regulatory TFs, and genes that regulate mitotic spindle function. As cells progress through the
45 cell cycle, Hcm1 is activated by multisite phosphorylation by cyclin dependent kinase (CDK) [18].
46 CDK phosphorylates eight sites in the Hcm1 transactivation domain (TAD) to stimulate its activity
47 and a three site phosphodegron in the N-terminus to trigger proteasomal degradation.
48 Immediately following exposure to $CaCl_2$ or LiCl stress, two stressors that activate CN, CDK
49 activity decreases, the activating phosphates on Hcm1 are removed by CN, and expression of

50 Hcm1 target genes decreases [14,15,19]. Whether or not Hcm1 inactivation is critical for cells to
51 adapt and survive in the face of chronic stress is unknown.

52 Mutations within the Hcm1 TAD have been used to study the consequences of
53 phosphorylation. Phosphomimetic mutations at all CDK phosphosites in the TAD generate a
54 constitutively active protein that leads to increased expression of Hcm1 target genes [18]. In
55 normal growth conditions this mutant provides a fitness advantage to cells, rendering them more
56 fit than wild type (WT) [15,20]. This is a surprising result because advantageous mutations are
57 expected to be selected for during evolution. However, the fact that activating phosphates are
58 removed by CN when cells are faced with stress suggests that dephosphorylation and inactivation
59 of Hcm1 may be necessary for cells to survive in stressful environments.

60 Here, we investigated this possibility and found that cells expressing a constitutively active,
61 phosphomimetic Hcm1 mutant lose their fitness advantage when they proliferate in LiCl stress for
62 up to 30 generations. To determine the optimal level of Hcm1 activity for fitness in this
63 environment, we screened a collection of Hcm1 mutants that encompass all possible
64 combinations of non-phosphorylatable and phosphomimetic mutations in the TAD, representing
65 the entire spectrum of possible activity levels. Surprisingly, this screen revealed that almost all
66 mutants were less fit, relative to WT, when growing in stress compared to stress-free conditions.
67 Moreover, Cks1-priming sites that stimulate Hcm1 activity by promoting phosphorylation by CDK
68 became more important for fitness when cells were grown in chronic stress. Finally, mutants that
69 have increased Hcm1 activity because proteasomal degradation is blocked, but retain dynamic
70 phosphoregulation of the TAD, upregulated Hcm1 target gene expression to a greater extent and
71 were more fit than WT cells in chronic stress. These results demonstrate that simple Hcm1
72 inactivation is not the mechanism by which cells survive in chronic stress; instead, dynamic
73 regulation of the Hcm1 activity – obtained through a combination of phosphorylation by CDK and
74 dephosphorylation by CN – is critical to maintain fitness.

75

76 **Results**

77

78 **Expression of a phosphomimetic Hcm1 mutant decreases fitness in LiCl stress**

79 CDK phosphorylates eight sites in the Hcm1 TAD to activate the protein during an unperturbed
80 cell cycle [18] . When cells are exposed to a CN-activating stressor such as $CaCl_2$ or LiCl, these
81 phosphates are removed by the phosphatase CN [15] (Fig 1A). This dephosphorylation occurs
82 rapidly after exposure to LiCl [15] and, notably, Hcm1 remains in a hypophosphorylated state after
83 cells adapt to LiCl stress and resume cycling (Fig 1B). To determine if dephosphorylation of Hcm1
84 is necessary for cells to survive when faced with chronic LiCl stress, we utilized a constitutively
85 active phosphomimetic Hcm1 mutant, Hcm1-8E, in which each CDK site in the TAD is mutated
86 to two glutamic acids (S/T-P to E-E) to mimic the charge of a phosphate [18,20]. The Hcm1-8E
87 protein is more active than WT Hcm1 and, as a result, confers a fitness advantage to cells in a
88 competitive growth assay in optimal growth conditions [15,20]. To determine the consequence of
89 elevated Hcm1 activity in stress, we used the same competitive growth assay to compare the
90 fitness of cells expressing Hcm1-8E to cells expressing WT Hcm1, in the presence or absence of
91 LiCl (Fig 1C-1D, S1A-S1C Fig). As previously shown [20], *hcm1-8E* cells exhibited a fitness
92 benefit in the absence of stress (Fig 1C). However, *hcm1-8E* cells lost their fitness advantage and
93 displayed a modest fitness defect when cultured in medium containing LiCl (Fig 1D), supporting
94 the possibility that cells need to inactivate Hcm1 to survive in the presence of chronic LiCl stress.

95

96 **Hcm1 mutants with fixed phosphorylation states are less fit in LiCl stress**

97 Hcm1 retains some phosphorylation when cells are grown for three days in LiCl (Fig 1B),
98 suggesting that some activity may remain, and that a reduced level of Hcm1 activity might be
99 optimal in stress. To test this hypothesis, we employed Phosphosite Scanning, a recently

100 developed approach that can simultaneously determine the effects of hundreds of phosphosite
101 mutations on cellular fitness [20]. Phosphosite scanning was previously used to screen a
102 collection of Hcm1 mutants in which each CDK phosphosite (S/T-P) in the TAD is mutated to an
103 unphosphorylatable alanine (A-P) or two glutamic acids (E-E), in all possible combinations (A/E
104 library, Fig 2A) [20]. In unstressed growth conditions, fitness values conferred by these Hcm1
105 mutants are highly correlated with the activity of each mutant and this collection of mutants
106 represents the entire continuum of possible Hcm1 activities, from the completely inactive Hcm1-
107 8A mutant (with all phosphosites mutated to A-P) to the Hcm1-8E mutant that has increased
108 activity relative to WT [20]. To determine the optimal amount of activity in stress, we used the
109 same Phosphosite Scanning approach and screened the Hcm1 A/E library in control and LiCl
110 containing media in parallel (Fig 2B).

111 As in the previous study, the Hcm1 A/E library was transformed into a strain where the
112 genomic copy of Hcm1 was expressed from a galactose-inducible promoter. At the start of the
113 screen, cells growing in galactose were diluted into control medium or medium containing LiCl
114 and expression of WT Hcm1 was shut off by adding dextrose (S1E Fig), ensuring that all Hcm1
115 protein in the cells was derived from the plasmid library (Fig 2B). Cultures were periodically
116 sampled and diluted over the course of 72 hours, and the relative abundance of each mutant was
117 tracked via sequencing, as described previously [20]. Unlike the previous study where cells were
118 diluted every 12 hours to maintain logarithmic growth, cells were diluted every 24 hours, which
119 allowed cells in control conditions to approach saturation and exit the cell cycle (S1D Fig).
120 However, Hcm1 expression resumed following each dilution when cells reentered the cell cycle
121 (S1E Fig), and selection coefficients of mutants screened in control conditions using 12- and 24-
122 hour intervals were highly correlated (S2A-C Fig). Thus, the modified screening protocol
123 accurately reflects the relative fitness values of Hcm1 mutants.

124 We first investigated how overall fitness was impacted when cells were growing in stress.
125 Selection coefficients of each mutant in LiCl-containing medium were directly compared with
126 those from control medium (Fig 2C). Surprisingly, although there was a strong correlation between
127 selection coefficients in the two environments, almost all mutants showed a stronger reduction in
128 fitness, relative to WT, in LiCl conditions than they exhibited in control conditions. This effect was
129 most severe for mutants with greatest number of phosphomimetic (activating) mutations, whereas
130 mutants that had two or fewer phosphomimetic mutations were most similar between control and
131 LiCl media (Fig 2D, S2D Fig). Notably, although the *hcm1-8E* mutant displayed a modest fitness
132 defect in pairwise competition assays carried out in LiCl (Fig 1D), it had a slight fitness advantage
133 in pooled screens (Fig 2D, mutant with eight E substitutions). This observation is consistent with
134 previous findings that pooled screens result in higher selection coefficients than pairwise
135 competition assays and is likely due to technical differences in the experimental approach [20].
136 However, the *hcm1-8E* mutant fitness advantage was modest in pooled LiCl screens and
137 decreased in LiCl compared to control conditions. These data demonstrate that, contrary to our
138 expectation, Hcm1 activity is required for fitness in stress. However, the most highly active
139 mutants exhibit reductions in fitness compared to control growth conditions.
140 Next, we wanted to determine how individual TAD phosphosites impact cellular fitness in
141 LiCl stress. To do this, we compared the selection coefficients of all mutants that had either a
142 non-phosphorylatable alanine (A) or two glutamic acids (E) at each site. In both control and LiCl
143 conditions, a phosphomimetic mutation at any site increased fitness relative to an alanine
144 substitution at the same site (Fig 2E-2F, compare red and blue boxes). Notably, mutations at sites
145 T460 and S471 had the greatest effect on fitness in both conditions, consistent with previous
146 measurements in the absence of stress [20]. Together, these data show that when
147 phosphorylation patterns of Hcm1 are fixed because all sites are changed to either
148 phosphodeficient or phosphomimetic amino acids, the fitness of almost all mutants decreases in

149 stress relative to WT. This raises the possibility that it is not inactivation of Hcm1 that is important
150 for cells to maintain fitness in stress, but rather dynamic regulation conferred by phosphorylation
151 and dephosphorylation of the TAD.
152
153 **Requirement for Cks1-dependent priming in elevated in stress**
154 If dynamic regulation of Hcm1 is important for cells to survive in stress, we hypothesized that
155 mechanisms that enhance phosphorylation by CDK would be more important in stress. One
156 mechanism that promotes phosphorylation by CDK is kinase priming facilitated by the CDK
157 accessory subunit Cks1. Cks1 binds to phosphorylated threonines at the N-terminal end of a
158 multisite phosphorylated domain and promotes phosphorylation of CDK sites that are C-terminal
159 to its binding site [21,22] . Importantly, Phosphosite Scanning can reveal Cks1-dependent
160 regulation. By screening libraries that include WT phosphosites in combination with
161 phosphodeficient or phosphomimetic mutations it is possible to identify how a mutation at one site
162 (either an unphosphorylatable alanine or glutamic acids, which mimic the charge of a phosphate
163 but don't facilitate Cks1 binding) influences phosphorylation at other sites [20]. Therefore, we
164 screened two additional libraries of Hcm1 mutants to investigate Cks1-dependent priming: one in
165 which all phosphosites are either WT or a non-phosphorylatable alanine (WT/A library, Fig 3A);
166 and one in which all phosphosites are either WT or phosphomimetic (WT/E library, Fig 4A) [20].
167 The fitness of all mutants was compared between control conditions and LiCl conditions, as
168 described above.
169 First, we performed Phosphosite Scanning of the WT/A library in control and LiCl stress.
170 Similar to the A/E screen, selection coefficients for all mutants were correlated between control
171 and LiCl stress, however all scores were reduced in LiCl compared to control (Fig 3B). Moreover,
172 alanine substitutions in an otherwise WT background (the W/A library) reduced fitness to a greater
173 extent than observed when the same alanine substitutions were included an otherwise

174 phosphomimetic background (the A/E library; compare Fig 3B with Fig 2C), which is consistent
175 with Hcm1 regulation by Cks1 [20]. Since Cks1 can only bind to phosphothreonine [21,22], alanine
176 substitutions reduce activity in two ways: first, activity is directly reduced because alanines cannot
177 be phosphorylated and provide the charge conferred by a phosphate and second, activity is
178 indirectly decreased because alanines cannot interact with Cks1 and thereby reduce
179 phosphorylation of more C-terminal WT sites in the domain. Despite the decreased fitness of all
180 mutants in the WT/A library, fitness generally increased with the number of WT sites in any given
181 mutant (Fig 3C), and a WT site was more advantageous than an alanine at each position (Fig 3D-
182 3E), in both control and LiCl conditions. These results support the conclusion that phosphorylation
183 at each site in the TAD contributes to Hcm1 activity in both control and stress conditions.

184 We further explored the contribution of Cks1 priming sites to fitness in stress by screening
185 the WT/E library (Fig 4A). Like alanine mutations, phosphomimetic (E-E) mutations cannot serve
186 as Cks1 priming sites. Because of this, E-E substitutions effectively behave as separation of
187 function mutations: they contribute to Hcm1 activation because they are charged, but are unable
188 to act as Cks1 priming sites, so they impair phosphorylation of more C-terminal WT sites in the
189 TAD. The cumulative effect of these mutations is evident when comparing selection coefficients
190 of WT/E mutants in control and LiCl conditions (Fig 4B). Whereas most mutants in this collection
191 are more fit than WT in control conditions, most mutants become less fit than WT in stress (Fig
192 4B, lower right quadrant). The subset of mutants that remained more fit than WT in stress included
193 most mutants that have phosphomimetic mutations at T460 and S471 (Fig 4B, red circles), likely
194 because this group of mutants does not depend on Cks1 priming to facilitate the phosphorylation
195 of these two sites that have the greatest impact on Hcm1 activity (Fig 2E-2F). Notably, in the
196 WT/E library, fitness did not increase with the number of phosphomimetic mutations when cells
197 were growing in LiCl (Fig 4C), suggesting that priming by Cks1 is of increased importance when
198 cells are growing in stress.

199 To further investigate the need for Cks1 priming, we analyzed the fitness of
200 phosphomutants based on their genotype at each site. In non-stress conditions, if a
201 phosphomimetic mutation has a negative effect and confers a reduced selection coefficient
202 compared to the WT CDK site, it suggests that position functions as a priming site [20]. For
203 example, in control media mutants that are phosphomimetic at site 428 are slightly less fit than
204 mutants that are WT at the same site (Fig 4D), whereas phosphomimetic mutations at site 428
205 increase fitness when compared to alanine mutations in the A/E library (Fig 2E). This difference
206 indicates that site 428 is a Cks1 priming site [20]. Notably, the deleterious fitness effect of this
207 phosphomimetic mutation was amplified in LiCl stress, and there was a similar reduction in fitness
208 among mutants that are phosphomimetic at site 440 (Fig 4E). Interestingly, mutants that were
209 phosphomimetic at two additional sites, 479 and 486, also showed a reduction in fitness relative
210 to mutants that are WT at the same sites in LiCl. Since these phosphomimetic mutations improved
211 or had little effect on fitness in control conditions (Fig 4D), suggesting that these may be additional
212 Cks1 priming sites within the Hcm1 TAD that only become important for fitness in stress. In fact,
213 mutants with phosphomimetic mutations at either T428 and T440 or T479 and T468 displayed
214 significantly reduced fitness in stress compared to mutants with WT sites, despite equivalent
215 fitness in control conditions (Fig 4F). The increased importance of Cks1-dependent priming
216 supports the conclusion that dynamic phosphorylation of the Hcm1 TAD is critical for fitness when
217 cells are challenged with LiCl stress.
218

219 **Dynamic phosphorylation of the Hcm1 TAD is required for fitness in stress**

220 If the *hcm1-8E* mutant is less fit in stress because its phosphorylation cannot be dynamically
221 regulated, and not because it has increased activity, then an alternative mutant in which Hcm1
222 activity is increased by a different mechanism might not exhibit reduced fitness in stress. To test
223 this possibility, we examined the fitness of *hcm1-3N* mutant cells. Hcm1-3N contains three alanine

224 substitutions in the N-terminal phosphodegron that prevent proteasomal degradation and stabilize
225 the protein [18], thereby increasing Hcm1 activity without perturbing TAD phosphorylation
226 dynamics (Fig 5A). First, we compared the activity of the Hcm1 mutants directly, by expressing
227 each mutant in an *hcm1Δ* reporter strain, where two copies of the Hcm1-responsive element from
228 the *WHI5* promoter drive GFP expression. Notably, Hcm1-3N was more active than WT Hcm1,
229 although it was less active than Hcm1-8E (Fig 5B). Despite this difference, both *hcm1-3N* and
230 *hcm1-8E* cells exhibited similar increases in fitness in the absence of stress (Fig 5C, 1C, 5E)
231 [15,20]. If dynamic regulation of the Hcm1 TAD is important for fitness in stress, *hcm1-3N* cells
232 should differ from *hcm1-8E* and retain their fitness advantage.

233 To test this hypothesis, pairwise competition assays were carried out between *hcm1-3N*
234 and WT cells in control and LiCl containing medium. Notably, in contrast to the decreased fitness
235 observed in *hcm1-8E* cells challenged with LiCl stress (Fig 1D, 5E), the fitness benefit in *hcm1-*
236 *3N* cells was enhanced under stress conditions (Fig 5D-5E). To compare these effects directly,
237 these two sets of mutations were combined to generate a stable, constitutively active mutant
238 (*hcm1-3N8E*, Fig 5A-5B). In a pairwise competition assay, *hcm1-3N8E* cells had similar fitness
239 as *hcm1-3N* cells in control conditions (Fig 5F), as previously reported [20]. However, *hcm1-3N8E*
240 cells were less fit than *hcm1-3N* in LiCl stress (Fig 5G). Therefore, preventing dynamic
241 phosphorylation of the Hcm1-3N protein reverses the fitness benefit provided by its stabilization
242 and increased expression in stress.

243

244 **Frequency modulation enhances Hcm1 activity in stress**

245 When cells are continuously exposed to a CN-activating stress, cells experience bursts in
246 cytosolic Ca^{2+}, followed by pulses of CN activity [23,24]. This suggests that Hcm1 may undergo
247 pulses of inactivation in chronic stress, which are then reversed by CDK activity. For some TFs,
248 increasing the frequency of pulses of activation results in a greater induction of target gene

249 expression, compared to increasing the amplitude of TF activity [25,26]. Therefore, we considered
250 that Hcm1 may undergo pulses of activity in stress, through modulation of phosphorylation, which
251 in turn could further increase the expression of its target genes. If so, WT and *hcm1-3N* cells
252 should increase Hcm1 target gene expression in stress, compared to unstressed conditions,
253 whereas *hcm1-8E* and *hcm1-8E3N* should not.

254 To test this hypothesis, we evaluated the activity of each mutant in the Hcm1 reporter
255 strain described above, in control and LiCl stress conditions. Strains were passaged in
256 monoculture, using the same dilution protocol that was employed for fitness assays, and
257 GFP levels were measured using both flow cytometry and Western blotting after 40 hours of
258 growth. As predicted, Hcm1-3N exhibited a significant increase in activity under stress, whereas
259 Hcm1-8E and Hcm1-3N8E showed either decreased or unchanged activity (Fig 6A, S3A-S3B Fig).
260 The WT protein also appeared more active under stress based on GFP levels detected by
261 Western blot (S3B Fig). However, flow cytometry revealed a modest fluorescence increase in
262 both WT and EV cells (Fig 6A, S3A Fig). Since no GFP protein was detected by Western blot in
263 EV cells, we conclude that the fluorescence increase may be due to a slight Hcm1-independent
264 increase in autofluorescence under stress. Notably, the increased activity of WT and Hcm1-3N
265 could not be attributed to changes in Hcm1 protein levels (S3B Fig) or differences in the proportion
266 of cells in S-phase (S3C Fig). These data support the model that pulses of activation increase
267 Hcm1 target gene expression.

268 We also examined whether Hcm1 mutants could enhance proliferation by comparing
269 population growth when the different Hcm1 proteins were expressed in the *hcm1Δ* reporter strain
270 during the 40-hour time course. In the absence of stress, all mutants supported proliferation as
271 well as WT Hcm1, whereas empty vector (EV) cells that do not express Hcm1 exhibited a
272 proliferation defect (Fig 6B). In contrast, mutants differentially affected proliferation when grown
273 in stress. Although all strains underwent fewer doublings in stress, strains expressing WT, Hcm1-

274 8E and Hcm1-3N8E were more similar to EV cells, whereas Hcm1-3N cells displayed a
275 proliferative advantage (Fig 6C). These results support the conclusions from pairwise competition
276 assays (Fig 1C-1D, Fig 5C-5G) and show that Hcm1-3N expression provides a fitness advantage
277 in stress.

278 We next examined how Hcm1 mutants impact the expression of endogenous Hcm1 target
279 genes in chronically stressed cells. Hcm1 only activates target gene expression during S-phase,
280 so the clearest way to examine the effect of Hcm1 mutants is to compare target gene expression
281 in S-phase synchronized cells [18] . However, we found that after cells have adapted to growing
282 in LiCl, they do not release synchronously from a G1 arrest (S4A Fig), making it difficult to quantify
283 gene expression specifically in S-phase. Therefore, we quantified target gene expression by
284 sequencing mRNA from asynchronous cells that were grown in control medium or LiCl for 40
285 hours. Because the experiment was performed in asynchronous cultures, where only ~16% of
286 cells are in S-phase (S4B Fig), we observed modest fold change differences between wild type
287 and mutant strains for individual Hcm1 target genes (S3 Dataset). For this reason, we used Gene
288 Set Enrichment Analysis (GSEA) to examine changes in expression of Hcm1 target genes as a
289 group. GSEA revealed that Hcm1 targets were collectively expressed at elevated levels in both
290 *hcm1-3N* and *hcm1-8E* mutants compared to WT in control conditions, confirming that the two
291 mutants exhibit a similar increase in activity (Fig 6D, a negative normalized enrichment score
292 (NES) indicates lower expression in WT compared to mutant). However, when cells were grown
293 in LiCl, Hcm1 target genes increased in expression in *hcm1-3N* cells, but not in *hcm1-8E* cells.
294 Moreover, target genes were more highly expressed in *hcm1-3N* cells than *hcm1-8E* cells when
295 they were directly compared (Fig 6D, a positive NES indicates higher expression in *hcm1-3*N
296 compared to *hcm1-8E*). These results demonstrate that dynamic phosphorylation of Hcm1 in
297 stress increases expression of Hcm1 target genes and suggests that expression of these genes
298 promotes fitness in stress.

299

300 **Discussion**

301 Immediately upon exposure to an environmental stressor, cells rewire many cellular pathways to
302 promote stress resistance and long-term survival. A conserved feature of this acute response is
303 the inactivation of cell cycle-regulatory TFs and downregulation of their target genes. Although
304 cell cycle arrest is not required for the execution of the acute stress response [27], it is possible
305 that arrest and/or downregulation of cell cycle-regulatory genes is important for adaptation and
306 survival after cells resume proliferation in the new environment. In support of this possibility, we
307 found that expression of the Hcm1-8E phosphomimetic mutant, which cannot be
308 dephosphorylated and inactivated, reduces fitness in chronic LiCl stress (Fig 1D). However,
309 several pieces of evidence argue that simple Hcm1 inactivation does not promote fitness in stress,
310 but rather its activity must be toggled on and off to maximally activate target gene expression and
311 ensure fitness. First, almost all Hcm1 phosphosite mutants that retain activity but have fixed
312 phosphorylation states are less fit, relative to WT, in LiCl than control conditions (Fig 2C). This
313 includes mutants that have WT-like activity, as well as those that have increased activity
314 compared to WT. Second, TP motifs that function as Cks1 priming sites to promote
315 phosphorylation by CDK are of greater importance in stress (Fig 4F), which suggests that
316 increased CDK-dependent phosphorylation is required to counteract CN-dependent
317 dephosphorylation. This is seen for T428 and T440, which are previously characterized Cks1
318 priming sites [20], as well as two putative Csk1 priming sites T479 and T486, which are of
319 increased importance only in stress. Finally, cells expressing the Hcm1-3N protein, which has
320 increased activity because it is stabilized but retains phosphorylation-dependent activation [20],
321 promotes the highest level of target gene expression and confers a fitness advantage in LiCl
322 stress (Fig 6D, 5E). Together, these data demonstrate that Hcm1 activity is required for fitness in
323 stress, and that the ability to add and remove phosphates is critical for maximal activity.

324 Dynamic regulation by phosphorylation is a recognized feature of many TFs, most notably
325 TFs that respond to stress. In mammalian cells pulsatile nuclear localization and activation of
326 NFAT [28], p53 [29–31] and NFκB [32–35] lead to an altered transcriptional output in response to
327 different signals. In budding yeast, at least ten TFs display pulsatile nuclear localization in
328 response to specific cues, thereby increasing frequency of their activation [36]. In the case of the
329 stress-activated TF Msn2, exposure to distinct stressors triggers either sustained or pulsatile
330 Msn2 nuclear localization [37], resulting in expression of distinct groups of target genes belonging
331 to different promoter classes [25,26]. Notably, the CN-regulated TF Crz1 also exhibits pulsative
332 activation via regulation of its nuclear localization [23,24]. When cells are exposed to continuous
333 extracellular $CaCl_2$, the frequency of cytosolic Ca^{2+} pulses increases, and these are followed by
334 pulses of CN activation. CN then dephosphorylates Crz1, leading to pulses of nuclear localization
335 and target gene activation. Importantly, Hcm1 does not display pulses of nuclear localization [36],
336 instead we propose that its activation is controlled by pulses of phosphorylation. Since Hcm1 is
337 also a CN target, when cells are growing in LiCl stress pulses of CN activity are expected to
338 dephosphorylate and inactive Hcm1, which is then countered by CDK-dependent phosphorylation,
339 leading to restoration of Hcm1 activity. To our knowledge the only described mechanism of TF
340 frequency modulation is through changing TF localization, therefore dynamic phosphorylation of
341 a TAD represents a novel mechanism of controlling TF target gene expression in stress.
342 Dynamic phosphoregulation is likely to also control the activities of other CDK target
343 proteins in stress. In addition to CN, which antagonizes CDK as well as other kinases [13], the
344 cell cycle-regulatory phosphatase Cdc14 is activated during the stress response [38–40] and
345 could regulate phosphorylation dynamics. Moreover, a recent phosphoproteomic study monitored
346 proteome-wide phosphorylation after acute exposure to more than 100 stress conditions and
347 found that ~20% of phosphorylated proteins, including Hcm1, show a change in phosphorylation
348 after acute stress exposure [41]. Interestingly, the two Hcm1 phosphosites that changed most

349 frequently in that study were T479 and T486, which our data suggests may be Cks1-dependent
350 priming sites that are of increased importance in stress (Fig 5F). Notably, monitoring rapidly
351 changing phosphorylation patterns on individual proteins is not technically feasible, therefore
352 observations of pulsatile phosphorylation have largely been restricted to proteins where changes
353 in phosphorylation are measured indirectly by a change in localization [36]. Here, we show that
354 Phosphosite Scanning can be used to infer the importance of phosphorylation dynamics [20].
355 Screening mutants in which all sites are mutated to either non-phosphorylatable or
356 phosphomimetic mutations reveals the importance of being able to add and remove phosphates.
357 In addition, by screening mutants that combine phosphosite mutations and wild type sites,
358 Phosphosite Scanning can reveal whether priming sites for the CDK accessory subunit Cks1 are
359 important in stress, supporting the importance of dynamic phosphorylation. We anticipate that this
360 approach will enable the investigation of phosphorylation dynamics of other proteins and reveal
361 whether dynamic phosphorylation is a common mechanism that modulates protein function when
362 cells are growing in stressful environments.
363

364 **Materials and Methods**

365 **Yeast strains and plasmids**

366 All cultures were grown in rich medium (YM-1) or synthetic media lacking uracil (C-Ura) with 2%
367 dextrose or galactose. Cultures were grown at 30°C or 23°C, as indicated. A record of strains and
368 plasmids used in this study can be found in S1 and S2 Tables, respectively. To construct the
369 Hcm1 reporter strain, a synthetic DNA containing two copies of the previously characterized Hcm1
370 responsive element from the *WHI5* promoter [16] was cloned upstream of the minimal *GAL1*
371 promoter and GFP. This sequence was integrated into a silent region on chromosome VI [42],
372 and then introduced into an *hcm1Δ* background by genetic cross.

373

374 **Co-culture competition assays**

375 Pairwise competition assays were done as described in Conti et al. 2023 ([20] and S1A Fig).
376 Strains in which the endogenous copy of *HCM1* is regulated by a galactose inducible promoter
377 (*GAL1p-HCM1*) and expressing either WT or non-fluorescent GFP (GFP-Y66F) were transformed
378 with low-copy plasmids expressing WT or mutant *HCM1* from the *HCM1* promoter. Initially,
379 cultures were grown in synthetic media lacking uracil with 2% galactose to ensure expression of
380 *HCM1*. Logarithmic phase cells were equally mixed by adding one optical density (OD600) of
381 each strain to the same culture tube in a final volume of 10mL C-Ura with 2% galactose. To
382 determine the starting abundance of each strain, 0.15 optical densities were collected from the
383 co-culture tubes. Samples were pelleted by centrifugation, resuspended in 2mL sodium citrate
384 (50mM sodium citrate, 0.02% NaN_3, pH 7.4) and stored at 4°C pending analysis by flow cytometry.
385 To evaluate fitness in LiCl stress, co-cultures were diluted within a range of 0.005-0.04 optical
386 densities (OD_{600}) into synthetic media lacking uracil with 2% dextrose with or without 150mM LiCl
387 after mixing at the start of the experiment. Cultures were then sampled and diluted every 24 hours
388 for a total of 96 hours. Cultures reached saturation prior to dilution. At each timepoint, 0.15 optical
389 densities were collected, pelleted, and resuspended in 2mL sodium citrate, and stored at 4°C until
390 the conclusion of the experiment. Following the final timepoint, the percentage of GFP positive
391 cells was quantified in each sample using a Guava EasyCyte HT flow cytometer and GuavaSoft
392 software. 5000 cells were measured in all samples. Results were analyzed using FloJo software.
393 Averages of n=3-13 biological replicates are shown; exact number is indicated in the figure
394 legends. Selection coefficients for pairwise assays were calculated by calculating the slope of the
395 best fit line of log2 fold change in mutant fraction over time, relative to WT in the same experiment.
396 Control competitions were performed with WT (*HCM1*) cells expressing GFP or the non-

397 fluorescent mutant GFP (GFP-Y66F). Expression of these markers had no effect on fitness (S1B-
398 C Fig).

399

400 **Western blotting**

401 Yeast culture amounting to one optical density (OD600) was collected, pelleted by centrifugation,
402 and stored at -80°C prior to lysis. Cell pellets were lysed by incubation with cold TCA buffer (10mM
403 Tris pH 8.0, 10% trichloroacetic acid, 25mM ammonium acetate, 1mM EDTA) on ice for 10
404 minutes. Lysates were mixed by vortexing and pelleted by centrifugation at 16,000xg for 10
405 minutes at 4°C. The supernatant was aspirated, and cell pellets were resuspended in 75μL
406 resuspension solution (100mM Tris pH 11, 3% SDS). Lysates were incubated at 95°C for five
407 minutes then allowed to cool to room temperature for five minutes. Lysates were clarified by
408 centrifugation at 16,000xg for 30 seconds at room temperature. Supernatants were then collected,
409 transferred to a new tube and 25μL 4X SDS-PAGE sample buffer (250mM Tris pH 6.8, 8% SDS,
410 40% glycerol, 20% β-mercaptoethanol) was added. The samples were incubated at 95°C for five
411 minutes, then allowed to cool to room temperature and stored at -80°C.

412 For standard Western blots, resolving gels contain 10% acrylamide/bis solution 37.5:1,
413 0.375M Tris pH 8.8, 0.1% SDS, 0.1% ammonium persulfate (APS), 0.04%
414 tetremethylethylenediamine (TEMED). Phos-tag gels contain 6% acrylamide/bis solution 29:1,
415 386mM Tris pH 8.8, 0.1% SDS, 0.2% APS, 25μM Phos-tag acrylamide (Wako), 50μM manganese
416 chloride and 0.17% TEMED. All stacking gels contain 5% acrylamide/bis solution 37.5:1, 126mM
417 Tris pH 6.8, 0.1% SDS, 0.1% APS and 0.1% TEMED. All SDS-PAGE gels were run in 1X running
418 buffer (200mM glycine, 25mM Tris, 35mM SDS). Phos-tag gels were washed twice with 1X
419 transfer buffer containing 10mM EDTA for 15 minutes (150mM glycine, 20mM Tris, 1.25mM SDS,

420 20% methanol) and once with 1X transfer buffer for 10 minutes on a shaking platform with gentle
421 agitation. All gels were transferred to nitrocellulose in cold 1X transfer buffer at 0.45A for two
422 hours. After transfer, nitrocellulose membranes were blocked in a 4% milk solution for 30 minutes.

423 Western blotting was performed with primary antibodies that recognize a V5 epitope tag
424 (Invitrogen, 1:1000 dilution), PSTAIRE (P7962, Sigma, 1:10,000 dilution), G6PDH (A9521, Sigma,
425 1:10,000 dilution), and GFP (632381, Clontech, 1:1000). Primary antibody incubations were
426 performed overnight at 4°C. Importantly, molecular weight makers are not shown with Phos-tag
427 gels as they do not accurately reflect the molecular weight of proteins.

428

429 **Phosphosite Scanning screens**

430 Phosphosite scanning screens were carried out using pooled plasmid libraries that were
431 previously constructed and characterized [20], and transformed into a *GAL1p-HCM1* strain. A
432 plasmid expressing WT *HCM1* was added to all libraries for normalization. During transformation,
433 cells were cultured in YM-1 containing 2% galactose to maintain expression of endogenous *HCM1.*
434 Following transformation, cells were cultured overnight at 23°C in synthetic media lacking uracil
435 (C-Ura) with 2% galactose. After approximately 16 hours, an aliquot of transformed cells was
436 removed and plated on C-Ura to confirm a transformation efficiency of at least 10X library size.
437 Remaining cells were washed with 15mL C-Ura with 2% galactose five times, resuspended in
438 50mL C-Ura with 2% galactose and allowed to grow to logarithmic phase for approximately 48
439 hours at 30°C. The starting population was sampled to determine the initial abundance of each
440 mutant in the population prior to selection. Cell pellets amounting to 20 optical densities were
441 harvested, frozen on dry ice, and stored at -80°C prior to preparation of sequencing libraries. To
442 evaluate fitness in stress, cultures were then diluted into synthetic media lacking uracil with 2%

443 dextrose with or without 150mM LiCl after sampling at time zero. For all timepoints after time zero,
444 cells were diluted into a range of 0.08 and 0.1 optical densities in 10mL of the appropriate media.
445 Cultures were sampled and diluted as above every 24 hours for a total of 72 hours.

446

447 **Illumina sequencing library preps**

448 For analysis by sequencing, plasmids were recovered from the frozen samples using a YeaStar
449 Genomic DNA Kit (Zymo Research). Mutant *hcm1* sequence was amplified by PCR (21 cycles)
450 using plasmid specific primers and Phusion High-Fidelity DNA polymerase (New England Biolabs).
451 DNA fragments were purified from a 1% agarose gel using a QIAquick Gel Extraction Kit (Qiagen).
452 Barcoded TruSeq adapters were added to the mutant fragments by PCR (7 cycles) using primers
453 specific to the *HCM1* region fused to either the TruSeq universal adapter or to a unique TruSeq
454 indexed adapter. Sequences of oligonucleotides that were used in library construction can be
455 found in S3 Table. Barcoded fragments were purified from a 1% agarose gel as described above.
456 Pooled barcoded libraries were sequenced on a HiSeq4000 platform (Novogene) to obtain paired-
457 end 150 base pair sequencing reads. All sequencing data is available from the NCBI Sequencing
458 Read Archive under BioProject # PRJNA1117860.

459

460 **Phosphosite scanning data analysis**

461 Abundance of *HCM1* alleles was quantified by counting all paired-end sequencing fragments that
462 had an exact match to an expected sequence in both reads using a custom python script. Custom
463 scripts used to generate count tables are available on GitHub
464 (https://github.com/radio1988/mutcount2024/tree/main/AE_type) and Zenodo
465 (https://zenodo.org/records/13144766). Selection coefficients were calculated as the slope of the

466 log2 fraction of reads versus time for each mutant, normalized to the log2 fraction of reads versus
467 time of WT. All selection coefficients for all screens can be found in S1 Dataset. Box and whisker
468 plots were generated using GraphPad Prism software. In all box and whisker plots the black
469 center line indicates the median selection coefficient, boxes indicate the 25th-75th percentiles,
470 black lines represent 1.5 interquartile range (IQR) of the 25th and 75th percentile, black circles
471 represent outliers. Statistical analyses for all plots of Phosphosite Scanning data are included in
472 S2 Dataset.

473

474 **Hcm1 activity assays**

475 Hcm1 activity was measured by expressing different Hcm1 proteins in an *hcm1Δ* reporter strain
476 before or after exposure to stress. At the time of collection, strains were resuspended in (50mM
477 sodium citrate, 0.02% NaN_3, pH 7.4) and GFP levels in each cell were quantified using a Guava
478 EasyCyte HT flow cytometer and GuavaSoft software. 5000 cells were measured in all samples.
479 Mean fluorescence activity (MFI) was calculated using FloJo software. Additional aliquots of cells
480 were saved for analysis of cell cycle position by measuring DNA content, and for analysis of Hcm1
481 and GFP levels by Western blot.

482

483 **RNA purification**

484 Cells amounting to five optical densities were harvested, pelleted by centrifugation at 3000rpm
485 for three minutes, and stored at -80°C. Cell pellets were then thawed on ice, resuspended in
486 400μL AE buffer (50mM sodium acetate pH 5.3, 10mM EDTA), and moved to room temperature.
487 40μL 10% SDS and 400μL AE equilibrated phenol was added to each sample and thoroughly
488 mixed by vortexing for 30 seconds. Samples were heated to 65°C for eight minutes and frozen in

489 a dry ice and ethanol bath for five minutes. Organic and aqueous layers were separated by
490 centrifugation at max speed for eight minutes at room temperature. The aqueous layer was then
491 transferred to a new tube. To remove any residual phenol, 500μL phenol:chloroform:isoamyl
492 alcohol was added and thoroughly mixed by vortexing for 30 seconds. Samples were incubated
493 at room temperature for five minutes and the aqueous and organic layers were separated by
494 centrifugation at maximum speed for five minutes at room temperature. The aqueous layer was
495 transferred to a new tube (~450μL) and the nucleic acids were precipitated by adding 40μL 3M
496 NaOAc pH 5.2 and 1mL 100% ethanol. Samples were mixed by vortexing for 15 seconds and
497 frozen in a dry ice and ethanol bath until completely frozen. Samples were then centrifuged at
498 maximum speed for 10 minutes at 4°C. Supernatants were decanted and pellets washed with 80%
499 ethanol and centrifuged at maximum speed for two minutes at 4°C. Supernatants were removed,
500 pellets allowed to dry completely and resuspended in 50μL water. DNA was degraded by
501 treatment with DNaseI. Samples were transferred to PCR strip tubes, 10μL 10X DNaseI buffer,
502 2μL DNaseI and 38μL water was added to each sample, and the samples were mixed by vortexing.
503 Samples were incubated at 30°C for 30 minutes, then cooled to 4°C in a thermocycler. 1μL 0.5M
504 EDTA was added to each sample and mixed. Samples were then heated to 75°C for 10 minutes
505 and cooled to 4°C in a thermocycler. Purified RNA (100μL) was then transferred to a new tube
506 and precipitated by adding 10μL sodium acetate pH 5.2 and 250μL 100% ethanol, and frozen in
507 a dry ice and ethanol bath until completely frozen. RNA was then pelleted by centrifugation at
508 maximum speed for 15 minutes at 4°C. Supernatants were decanted, the pellets washed with 80%
509 ethanol, centrifuged at maximum speed for 2 minutes at 4°C. Supernatants were decanted and
510 pellets allowed to air dry. Purified RNA was resuspended in water. Three biological replicates
511 were performed. Library preparation and sequencing, including polyA mRNA selection, strand
512 specific library preparation, and paired-end 100 base pair sequencing, were performed by

513 Innomics/BGI Americas. All sequencing data is available in NCBI GEO and is accessible through
514 GEO accession number GSE276435.

515

516 **RNAseq analysis**

517 RNASeq analysis was performed with OneStopRNAseq [43]. Paired-end reads were aligned to
518 Saccharomyces_cerevisiae.R64-1-1, with 2.7.7a [44], and annotated with
519 Saccharomyces_cerevisiae.R64-1-1.90.gtf. Aligned exon fragments with mapping quality higher
520 than 20 were counted toward gene expression with featureCounts [45]. Differential expression
521 (DE) analysis was performed with DESeq2 [46]. Within DE analysis, 'ashr' was used to create
522 log2 Fold Change (LFC) shrinkage [47] for all possible comparisons of WT and mutant strains, in
523 both control and LiCl conditions. Significant DE genes (DEGs) were filtered with the criteria FDR
524 < 0.05. Gene set enrichment analysis was performed for Hcm1 targets genes using GSEA [48]
525 on the ranked LFC. LFC analyses and GSEA results are included in S3 Dataset.

526

527 **Analysis of cell cycle position by flow cytometry**

528 To analyze DNA content by flow cytometry, cells amounting to 0.15 optical densities were
529 collected, fixed in 70% ethanol and stored at 4°C. Cells were then pelleted by centrifugation at
530 3000rpm for three minutes, resuspended in 1mL sodium citrate buffer (50mM sodium citrate, 0.02%
531 NaN_3, pH 7.4) and sonicated. Samples were then pelleted by centrifugation, resuspended in 1mL
532 sodium citrate buffer containing 0.25mg/mL RNaseA, and incubated at 50°C for one hour. 12.5μL
533 10mg/mL Proteinase K was added to each tube and samples were incubated for an additional
534 hour at 50°C. Following incubation, 1mL sodium citrate buffer containing 0.4μL Sytox green was
535 added to each sample and samples were left at room temperature for 1 hour or 4°C overnight,

536 protected from light, for staining. DNA content was analyzed on a Guava EasyCyte HT flow
537 cytometer and GuavaSoft software. 5000 cells were measured in all samples. Results were
538 analyzed using FlowJo software. Percent cell cycle progression was calculated using the
539 following equation: % progression = ((H – 1C)/(2C-1C)) × 100, where H = histogram mean
540 fluorescence intensity (MFI), 1C = MFI of 1C DNA content peak, and 2C = MFI of2C DNA
541 content peak.

542

543 **Acknowledgements**

544 The authors thank Tom Fazzio and members of the Benanti lab for insightful discussions and
545 critical reading of the manuscript. This work was supported by National Institutes of Health grant
546 R35GM136280 to J.A.B.

547

548 **References**

549 1. Senft D, Ronai ZA. Adaptive Stress Responses During Tumor Metastasis and Dormancy.
550 Trends Cancer. 2016;2: 429–442. doi:10.1016/j.trecan.2016.06.004

551 2. Pizzinga M, Harvey RF, Garland GD, Mordue R, Dezi V, Ramakrishna M, et al. The cell
552 stress response: extreme times call for post-transcriptional measures. Wiley Interdiscip Rev:
553 RNA. 2020;11: e1578. doi:10.1002/wrna.1578

554 3. Park H-S, Lee SC, Cardenas ME, Heitman J. Calcium-Calmodulin-Calcineurin Signaling: A
555 Globally Conserved Virulence Cascade in Eukaryotic Microbial Pathogens. Cell Host Microbe.
556 2019;26: 453–462. doi:10.1016/j.chom.2019.08.004

557 4. Gasch AP, Spellman PT, Kao CM, Carmel-Harel O, Eisen MB, Storz G, et al. Genomic
558 Expression Programs in the Response of Yeast Cells to Environmental Changes. Mol Biol Cell.
559 2000;11: 4241–4257. doi:10.1091/mbc.11.12.4241

560 5. Causton HC, Ren B, Koh SS, Harbison CT, Kanin E, Jennings EG, et al. Remodeling of
561 Yeast Genome Expression in Response to Environmental Changes. Mol Biol Cell. 2001;12:
562 323–337. doi:10.1091/mbc.12.2.323

563 6. Yaakov G, Duch A, García-Rubio M, Clotet J, Jiménez J, Aguilera A, et al. The stress-
564 activated protein kinase Hog1 mediates S phase delay in response to osmostress. Molecular
565 biology of the cell. 2009;20: 3572–3582. doi:10.1091/mbc.e09-02-0129

566 7. Clotet J, Escoté X, Adrover MA, Yaakov G, Garí E, Aldea M, et al. Phosphorylation of Hsl1 by
567 Hog1 leads to a G2 arrest essential for cell survival at high osmolarity. EMBO J. 2006;25: 2338–
568 2346. doi:10.1038/sj.emboj.7601095

569 8. Flynn MJ, Harper NW, Li R, Zhu LJ, Lee MJ, Benanti JA. Calcineurin promotes adaptation to
570 chronic stress through two distinct mechanisms. Mol Biol Cell. 2024; mbcE24030122.
571 doi:10.1091/mbc.e24-03-0122

572 9. Li S, Giardina DM, Siegal ML. Control of nongenetic heterogeneity in growth rate and stress
573 tolerance of Saccharomyces cerevisiae by cyclic AMP-regulated transcription factors. PLoS
574 Genet. 2018;14: e1007744. doi:10.1371/journal.pgen.1007744

575 10. Bergen AC, Kocik RA, Hose J, McClean MN, Gasch AP. Modeling single-cell phenotypes
576 links yeast stress acclimation to transcriptional repression and pre-stress cellular states. Elife.
577 2022;11. doi:10.7554/elife.82017

578 11. Bonny AR, Kochanowski K, Diether M, El-Samad H. Stress-induced growth rate reduction
579 restricts metabolic resource utilization to modulate osmo-adaptation time. Cell Reports.
580 2021;34: 108854. doi:10.1016/j.celrep.2021.108854

581 12. Cyert MS, Philpott CC. Regulation of cation balance in Saccharomyces cerevisiae.
582 Genetics. 2013;193: 677–713. doi:10.1534/genetics.112.147207

583 13. Goldman A, Roy J, Bodenmiller B, Wanka S, Landry CR, Aebersold R, et al. The
584 Calcineurin Signaling Network Evolves via Conserved Kinase-Phosphatase Modules that
585 Transcend Substrate Identity. Mol Cell. 2014. doi:10.1016/j.molcel.2014.05.012

586 14. Leech CM, Flynn MJ, Arsenault HE, Ou J, Liu H, Zhu LJ, et al. The coordinate actions of
587 calcineurin and Hog1 mediate the stress response through multiple nodes of the cell cycle
588 network. Toczyski DP, editor. PLoS Genetics. 2020;16: e1008600-27.
589 doi:10.1371/journal.pgen.1008600

590 15. Arsenault HE, Roy J, Mapa CE, Cyert MS, Benanti JA. Hcm1 integrates signals from Cdk1
591 and Calcineurin to control cell proliferation. Molecular biology of the cell. 2015;26: 3570–3577.
592 doi:10.1091/mbc.e15-07-0469

593 16. Pramila T, Wu W, Miles S, Noble WS, Breeden LL. The Forkhead transcription factor Hcm1
594 regulates chromosome segregation genes and fills the S-phase gap in the transcriptional
595 circuitry of the cell cycle. Genes & Development. 2006;20: 2266–2278.
596 doi:10.1101/gad.1450606

597 17. Alvarez-Fernández M, Medema RH. Novel functions of FoxM1: from molecular mechanisms
598 to cancer therapy. Frontiers in oncology. 2013;3: 30. doi:10.3389/fonc.2013.00030

599 18. Landry BD, Mapa CE, Arsenault HE, Poti KE, Benanti JA. Regulation of a transcription
600 factor network by Cdk1 coordinates late cell cycle gene expression. The EMBO Journal.
601 2014;33: 1044–1060. doi:10.1002/embj.201386877

602 19. Flynn MJ, Benanti JA. Cip1 tunes cell cycle arrest duration upon calcineurin activation. Proc
603 National Acad Sci. 2022;119: e2202469119. doi:10.1073/pnas.2202469119

604 20. Conti MM, Li R, Ramos MAN, Zhu LJ, Fazzio TG, Benanti JA. Phosphosite Scanning
605 reveals a complex phosphorylation code underlying CDK-dependent activation of Hcm1. Nat
606 Commun. 2023;14: 310. doi:10.1038/s41467-023-36035-9

607 21. McGrath DA, Balog ERM, Kõivomägi M, Lucena R, Mai MV, Hirschi A, et al. Cks confers
608 specificity to phosphorylation-dependent CDK signaling pathways. Nature Structural &
609 Molecular Biology. 2013;20: 1407–1414. doi:10.1038/nsmb.2707

610 22. Kõivomägi M, Örd M, Iofik A, Valk E, Venta R, Faustova I, et al. Multisite phosphorylation
611 networks as signal processors for Cdk1. Nature Structural & Molecular Biology. 2013;20: 1415–
612 1424. doi:10.1038/nsmb.2706

613 23. Hsu IS, Strome B, Plotnikov S, Moses AM. A Noisy Analog-to-Digital Converter Connects
614 Cytosolic Calcium Bursts to Transcription Factor Nuclear Localization Pulses in Yeast. G3:
615 Genes, Genomes, Genet. 2019;9: 561–570. doi:10.1534/g3.118.200841

616 24. Cai L, Dalal CK, Elowitz MB. Frequency-modulated nuclear localization bursts coordinate
617 gene regulation. Nature. 2008;455: 485–490. doi:10.1038/nature07292

618 25. Hansen AS, O'Shea EK. Promoter decoding of transcription factor dynamics involves a
619 trade-off between noise and control of gene expression. Mol Syst Biol. 2013;9: 704–704.
620 doi:10.1038/msb.2013.56

621 26. Hansen AS, O'Shea EK. Limits on information transduction through amplitude and
622 frequency regulation of transcription factor activity. eLife. 2015;4: e06559.
623 doi:10.7554/elife.06559

624 27. Ho Y-H, Shishkova E, Hose J, Coon JJ, Gasch AP. Decoupling Yeast Cell Division and
625 Stress Defense Implicates mRNA Repression in Translational Reallocation during Stress.
626 Current Biology. 2018;28: 1–21. doi:10.1016/j.cub.2018.06.044

627 28. Yissachar N, Sharar Fischler T, Cohen AA, Reich-Zeliger S, Russ D, Shifrut E, et al.
628 Dynamic Response Diversity of NFAT Isoforms in Individual Living Cells. Mol Cell. 2013;49:
629 322–330. doi:10.1016/j.molcel.2012.11.003

630 29. Lahav G, Rosenfeld N, Sigal A, Geva-Zatorsky N, Levine AJ, Elowitz MB, et al. Dynamics of
631 the p53-Mdm2 feedback loop in individual cells. Nat Genet. 2004;36: 147–150.
632 doi:10.1038/ng1293

633 30. Batchelor E, Loewer A, Mock C, Lahav G. Stimulus-dependent dynamics of p53 in single
634 cells. Mol Syst Biol. 2011;7: 488–488. doi:10.1038/msb.2011.20

635 31. Purvis JE, Karhohs KW, Mock C, Batchelor E, Loewer A, Lahav G. p53 dynamics control
636 cell fate. Science (New York, NY). 2012;336: 1440–1444. doi:10.1126/science.1218351

637 32. Lee TK, Denny EM, Sanghvi JC, Gaston JE, Maynard ND, Hughey JJ, et al. A Noisy
638 Paracrine Signal Determines the Cellular NF-κB Response to Lipopolysaccharide. Sci Signal.
639 2009;2: ra65. doi:10.1126/scisignal.2000599

640 33. Ashall L, Horton CA, Nelson DE, Paszek P, Harper CV, Sillitoe K, et al. Pulsatile Stimulation
641 Determines Timing and Specificity of NF-κB-Dependent Transcription. Science. 2009;324: 242–
642 246. doi:10.1126/science.1164860

643 34. Tay S, Hughey JJ, Lee TK, Lipniacki T, Quake SR, Covert MW. Single-cell NF-κB dynamics
644 reveal digital activation and analogue information processing. Nature. 2010;466: 267–271.
645 doi:10.1038/nature09145

646 35. Lee REC, Qasaimeh MA, Xia X, Juncker D, Gaudet S. NF-κB signalling and cell fate
647 decisions in response to a short pulse of tumour necrosis factor. Sci Rep. 2016;6: 39519.
648 doi:10.1038/srep39519

649 36. Dalal CK, Cai L, Lin Y, Rahbar K, Elowitz MB. Pulsatile dynamics in the yeast proteome.
650 Current biology : CB. 2014;24: 2189–2194. doi:10.1016/j.cub.2014.07.076

651 37. Hao N, O'Shea EK. Signal-dependent dynamics of transcription factor translocation controls
652 gene expression. Nat Struct Mol Biol. 2012;19: 31–39. doi:10.1038/nsmb.2192

653 38. Reiser V, D'Aquino KE, Ee L-S, Amon A. The stress-activated mitogen-activated protein
654 kinase signaling cascade promotes exit from mitosis. Molecular biology of the cell. 2006;17:
655 3136–3146. doi:10.1091/mbc.e05-12-1102

656 39. Chasman D, Ho Y-H, Berry DB, Nemec CM, MacGilvray ME, Hose J, et al. Pathway
657 connectivity and signaling coordination in the yeast stress-activated signaling network.
658 Molecular systems biology. 2014;10: 759–759. doi:10.15252/msb.20145120

659 40. Tognetti S, Jiménez J, Viganò M, Duch A, Queralt E, Nadal E de, et al. Hog1 activation
660 delays mitotic exit via phosphorylation of Net1. Proceedings of the National Academy of
661 Sciences. 2020;1505: 201918308–8933. doi:10.1073/pnas.1918308117

662 41. Leutert M, Barente AS, Fukuda NK, Rodriguez-Mias RA, Villén J. The regulatory landscape
663 of the yeast phosphoproteome. Nat Struct Mol Biol. 2023;30: 1761–1773. doi:10.1038/s41594-
664 023-01115-3

665 42. Torres EM, Dephoure N, Panneerselvam A, Tucker CM, Whittaker CA, Gygi SP, et al.
666 Identification of aneuploidy-tolerating mutations. Cell. 2010;143: 71–83.
667 doi:10.1016/j.cell.2010.08.038

668 43. Li R, Hu K, Liu H, Green MR, Zhu LJ. OneStopRNAseq: A Web Application for
669 Comprehensive and Efficient Analyses of RNA-Seq Data. Genes-basel. 2020;11: 1165.
670 doi:10.3390/genes11101165

671 44. Dobin A, Davis CA, Schlesinger F, Drenkow J, Zaleski C, Jha S, et al. STAR: ultrafast
672 universal RNA-seq aligner. Bioinformatics. 2013;29: 15–21. doi:10.1093/bioinformatics/bts635

673 45. Liao Y, Smyth GK, Shi W. featureCounts: an efficient general purpose program for assigning
674 sequence reads to genomic features. Bioinformatics. 2014;30: 923–930.
675 doi:10.1093/bioinformatics/btt656

676 46. Love MI, Huber W, Anders S. Moderated estimation of fold change and dispersion for RNA-
677 seq data with DESeq2. Genome Biol. 2014;15: 550. doi:10.1186/s13059-014-0550-8

678 47. Stephens M. False discovery rates: a new deal. Biostat Oxf Engl. 2017;18: 275–294.
679 doi:10.1093/biostatistics/kxw041

680 48. Subramanian A, Tamayo P, Mootha VK, Mukherjee S, Ebert BL, Gillette MA, et al. Gene set
681 enrichment analysis: A knowledge-based approach for interpreting genome-wide expression
682 profiles. Proc National Acad Sci. 2005;102: 15545–15550. doi:10.1073/pnas.0506580102

683

684 **Figure Legends**

685 **Figure 1. Expression of a phosphomimetic Hcm1 mutant decreases fitness in LiCl stress**

686 (A) Hcm1 activity is regulated by cyclin-dependent kinase (CDK) and the phosphatase calcineurin
687 (CN). (B) Phos-tag and standard Western blots showing Hcm1 phosphorylation and expression
688 after the indicated number of hours in LiCl stress. Hcm1 was detected with an antibody that
689 recognizes a 3V5 tag, PSTAIRE is shown as a loading control. Representative blots from n=3
690 experiments are shown. (C-D) Strains with the indicated genotypes were co-cultured in control
691 media (C) or media with 150mM LiCl (D). Percentage of each strain was quantified by flow
692 cytometry at the indicated timepoints. An average of n=3 biological replicates is shown. Error bars
693 represent standard deviations.

694

695 **Figure 2. Phosphosite mutations in Hcm1 decrease fitness in stress.**

696 (A) Schematic depicting the Hcm1 A/E library. (B) Schematic of Phosphosite Scanning screens.
697 Plasmids expressing all 256 mutants in the A/E library, as well as WT *HCM1*, were transformed
698 into a strain in which expression of the genomic copy of *HCM1* is controlled by a galactose-
699 inducible promoter. The pooled population growing in galactose was diluted and split into dextrose
700 containing media (to shut-off expression of the endogenous copy of WT *HCM1*) with or without
701 150mM LiCl at the start of the experiment. (C) Scatterplot comparing average selection
702 coefficients for each mutant in the A/E library in control and LiCl media. Pearson correlation (r) is
703 indicated. (D-F) Box and whisker plots comparing the selection coefficients of different groups of
704 mutants. The black center line indicates the median selection coefficient, boxes indicate the 25th-
705 75th percentiles, whiskers represent 1.5 interquartile range (IQR) of the 25th and 75th percentile,
706 black circles represent outliers. In all panels, selection coefficients are an average of n=4
707 biological replicates. (D) shows selection coefficients in cells with the indicated number of
708 phosphomimetic mutations in control or LiCl conditions. (E-F) show selection coefficients of
709 mutants that are either phosphodead or phosphomimetic at each position, in control (E) or LiCl
710 containing medium (F). Statistics for panels D-F are included in S2 Dataset.
711
712 **Figure 3. All phosphosites in the Hcm1 TAD contribute to fitness in stress.**
713 (A) Schematic depicting the Hcm1 WT/A library. (B) Scatterplot comparing average selection
714 coefficients for each mutant in the WT/A library in control and LiCl media. Pearson correlation (r)
715 is indicated. (C-E) Box and whisker plots comparing the selection coefficients of different groups
716 of mutants. The black center line indicates the median selection coefficient, boxes indicate the
717 25th-75th percentiles, whiskers represent 1.5 interquartile range (IQR) of the 25th and 75th
718 percentile, black circles represent outliers. In all panels, selection coefficients are an average of
719 n=4 biological replicates. (B) shows selection coefficients in cells with the indicated number of WT
720 sites in control or LiCl conditions. (C-D) show selection coefficients of mutants that are either WT

721 (S or T) or alanine at each position, in control (C) or LiCl containing medium (D). Statistics for
722 panels C-E are included in Dataset S2.
723
724 **Figure 4. Elevated importance of processive Hcm1 phosphorylation in stress**
725 (A) Schematic depicting the Hcm1 WT/E library. (B) Scatterplot comparing average selection
726 coefficients for each mutant in the W/E library in control and LiCl media. Pearson correlation (r)
727 is indicated. Red represents mutants that are phosphomimetic at sites T460 and S471, blue
728 represents all other mutants. (C-F) Box and whisker plots comparing the selection coefficients of
729 different groups of mutants. The black center line indicates the median selection coefficient, boxes
730 indicate the 25th-75th percentiles, whiskers represent 1.5 interquartile range (IQR) of the 25th and
731 75th percentile, black circles represent outliers. In all panels, selection coefficients are an average
732 of n=4 biological replicates. (C) shows selection coefficients in cells with the indicated number of
733 phosphomimetic mutations in control or LiCl conditions. (D-E) show selection coefficients of
734 mutants that are either WT (S or T) or phosphomimetic at each position, in control (D) or LiCl
735 containing medium (E). (F) shows selection coefficients for mutants that are WT (TT) or
736 phosphomimetic (EE) at indicated positions. Statistics for panels C-F are included in Dataset S2.
737
738 **Figure 5. Dynamic phosphorylation of the Hcm1 TAD promotes fitness in stress.**
739 (A) Diagram of Hcm1 mutant proteins showing mutated phosphosites and impacts on protein
740 stability and phosphoregulation of the TAD region. nc, no change. (B) Mean Fluorescence
741 Intensity (MFI) of GFP expression in Hcm1 reporter strains expressing the indicated Hcm1
742 proteins or an empty vector (EV). An average of n=6 replicates is shown. Error bars represent
743 standard deviation. (C-D) *HCM1* and *hcm1-3N* strains were co-cultured in control media (C) or
744 media with 150mM LiCl (D). Percentage of each strain was quantified by flow cytometry at the

745 indicated timepoints. An average of n=13 biological replicates is shown. Error bars represent
746 standard deviations. (E) Comparison of selection coefficients of the indicated strains and growth
747 conditions, from pairwise assays shown in Figures 1C, 1D, 4B, and 4C. One-way ordinary ANOVA
748 with Šídák's multiple comparisons test was used to test significance, *p<0.0001. (F-G) *hcm1-3N*
749 and *hcm1-3N8E* strains were co-cultured in control media (F) or media with 150mM LiCl (G).
750 Percentage of each strain was quantified by flow cytometry at the indicated timepoints. An
751 average of n=13 biological replicates is shown. Error bars represent standard deviations.

752

753 **Figure 6. Dynamic phosphorylation increases Hcm1 activity in stress**

754 (A) Mean Fluorescence Intensity (MFI) of GFP expression in Hcm1 reporter strains expressing
755 the indicated Hcm1 proteins or an empty vector (EV), after 40 hours of growth in control medium
756 or medium with 150mM LiCl. An average of n=6 replicates is shown. Error bars represent standard
757 deviation. Two-way ANOVA with Šídák's multiple comparisons test was used to test significance,
758 *p<0.05. Representative histograms are shown in S3A Fig. (B-C) Cumulative generations of
759 strains from (A) over the 40-hour experiments. Shown is an average of n=6 replicates, errors bars
760 represent standard deviations. Strains grown in control conditions are shown in part (B). Strains
761 grown in LiCl stress are shown in part (C). (D) Normalized enrichment scores (NES) of Hcm1
762 target genes from GSEA analysis of the indicated comparisons. Asterisk (*) indicates FDR=0, ns
763 indicates not significant.

Figure 1

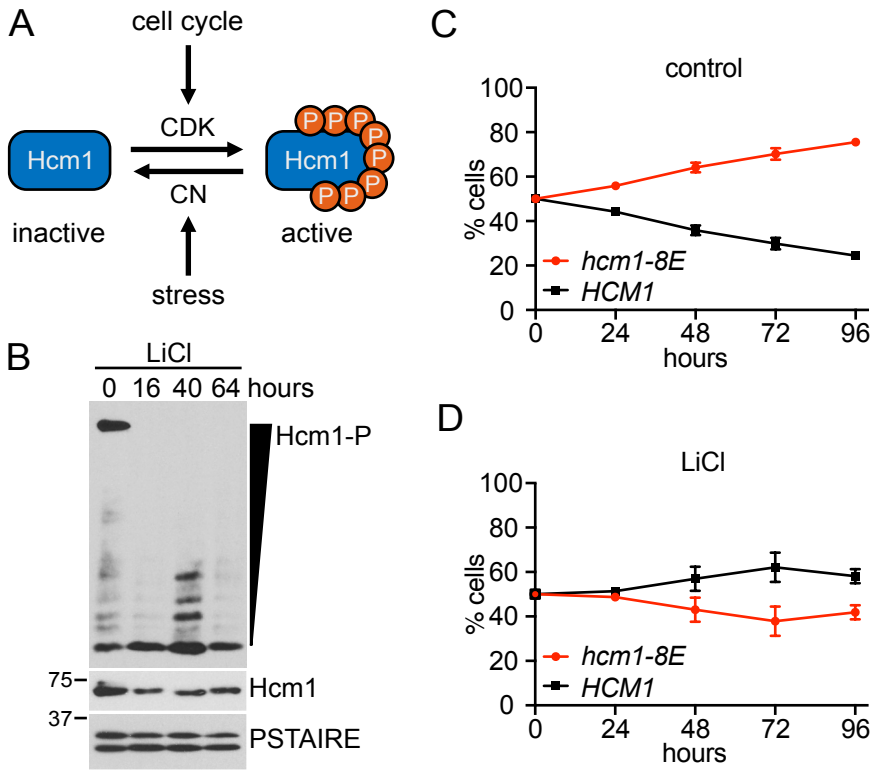
A
cell cycle
CDK
Hcm1
Hcm1
CN
inactive
active
stress
B
LiCl
0 16 40 64 hours
Hcm1-P
75
Hcm1
37
PSTAIRE
C
control
100
80
60
40
20
0
% cells
hcm1-8E
HCM1
0 24 48 72 96
hours
D
LiCl
100
80
60
40
20
0
% cells
hcm1-8E
HCM1
0 24 48 72 96
hours

Figure 2

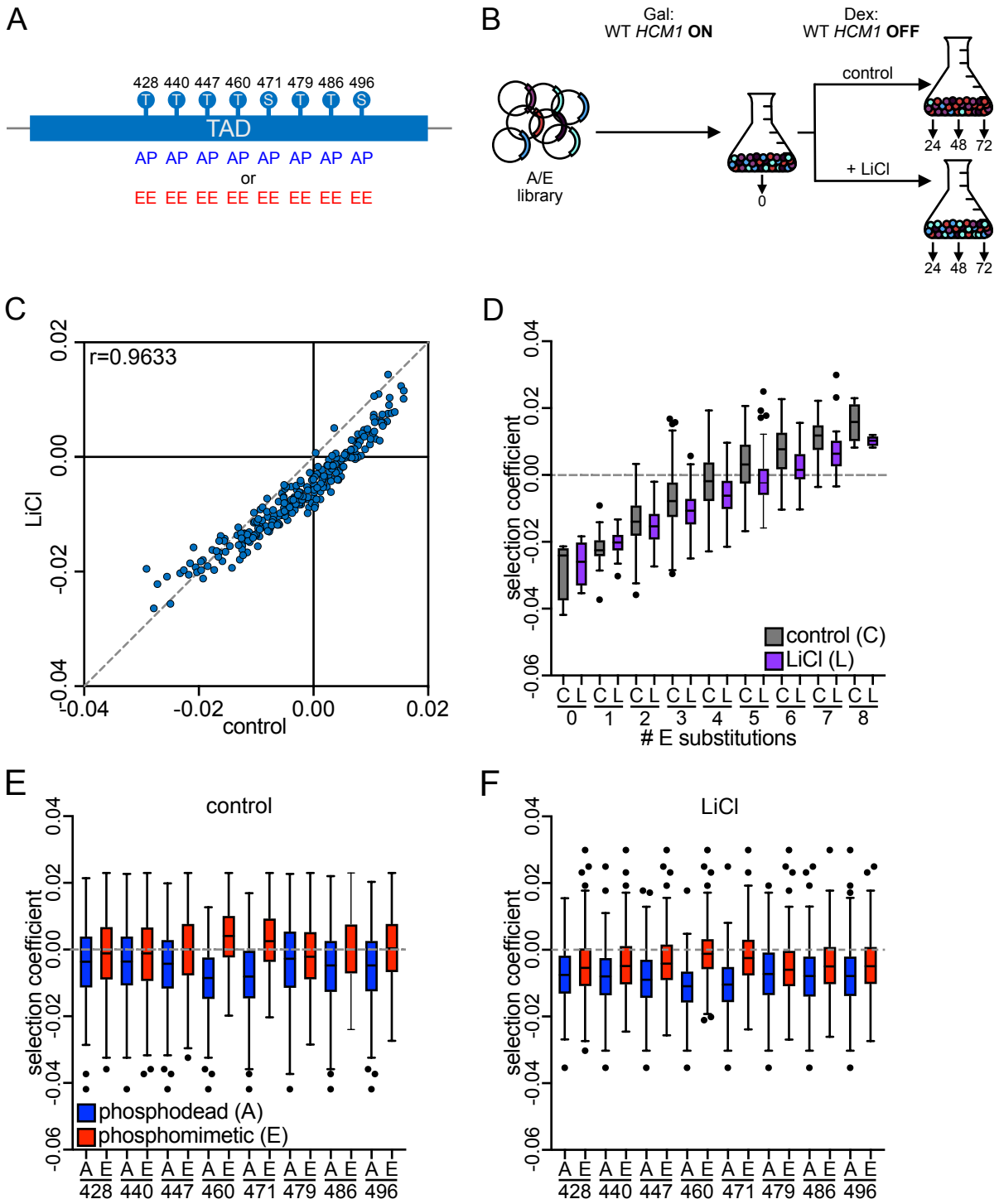
A
428 440 447 460 471 479 486 496
T T T T S T T S
TAD
AP AP AP AP AP AP AP AP
or
EE EE EE EE EE EE EE EE
B
Gal:
WT HCM1 ON
Dex:
WT HCM1 OFF
control
+ LiCl
A/E
library
0
24 48 72
24 48 72
C
r=0.9633
LiCl
control
D
selection coefficient
control (C)
LiCl (L)
E substitutions
E
control
selection coefficient
phosphodead (A)
phosphomimetic (E)
F
LiCl
selection coefficient

Figure 3

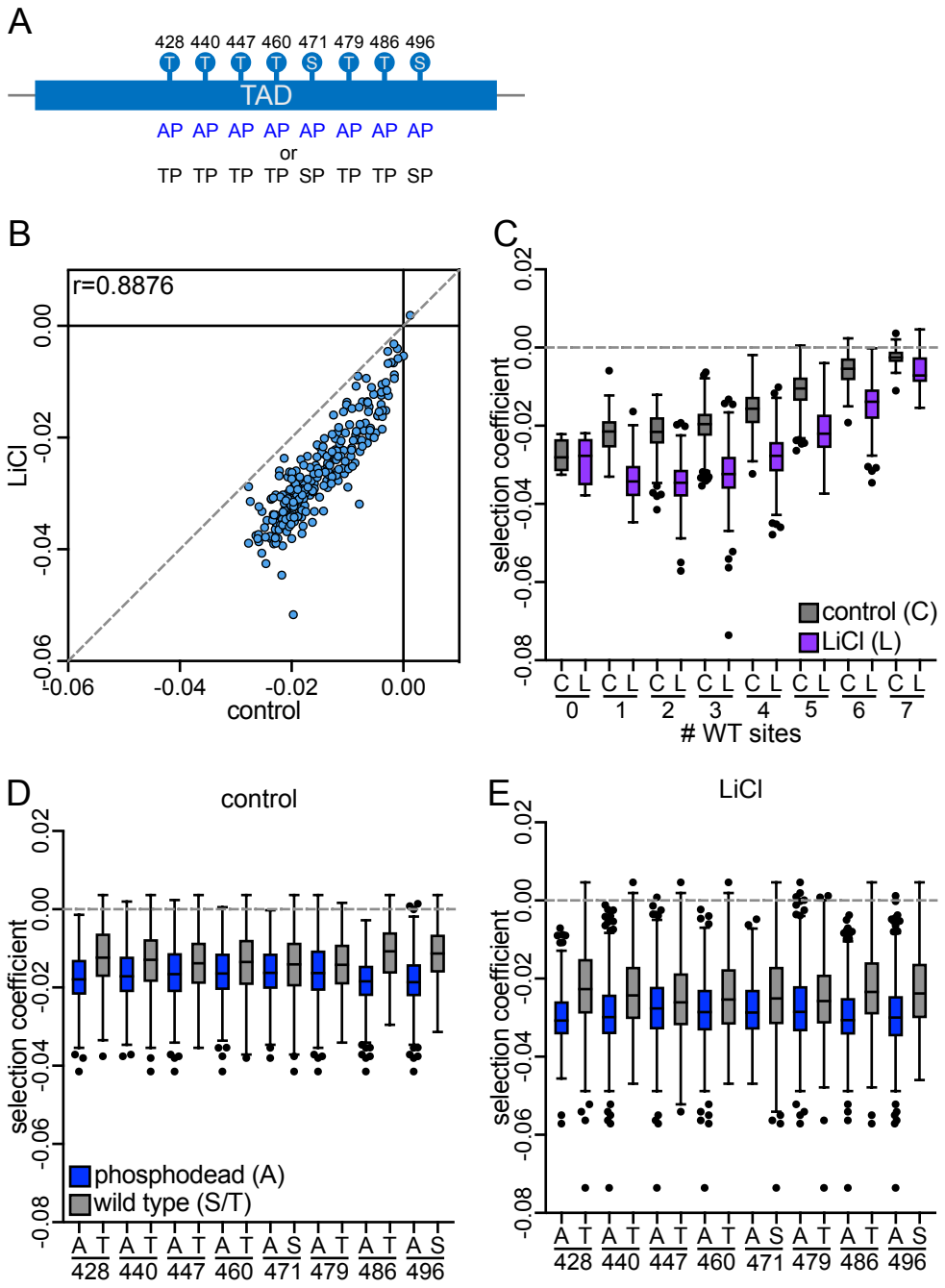
A
428 440 447 460 471 479 486 496
T T T T S T T S
TAD
AP AP AP AP AP AP AP AP
or
TP TP TP TP SP TP TP SP
B
r=0.8876
LiCl
control
C
selection coefficient
control (C)
LiCl (L)
WT sites
D
control
selection coefficient
phosphodead (A)
wild type (S/T)
E
LiCl
selection coefficient

Figure 4

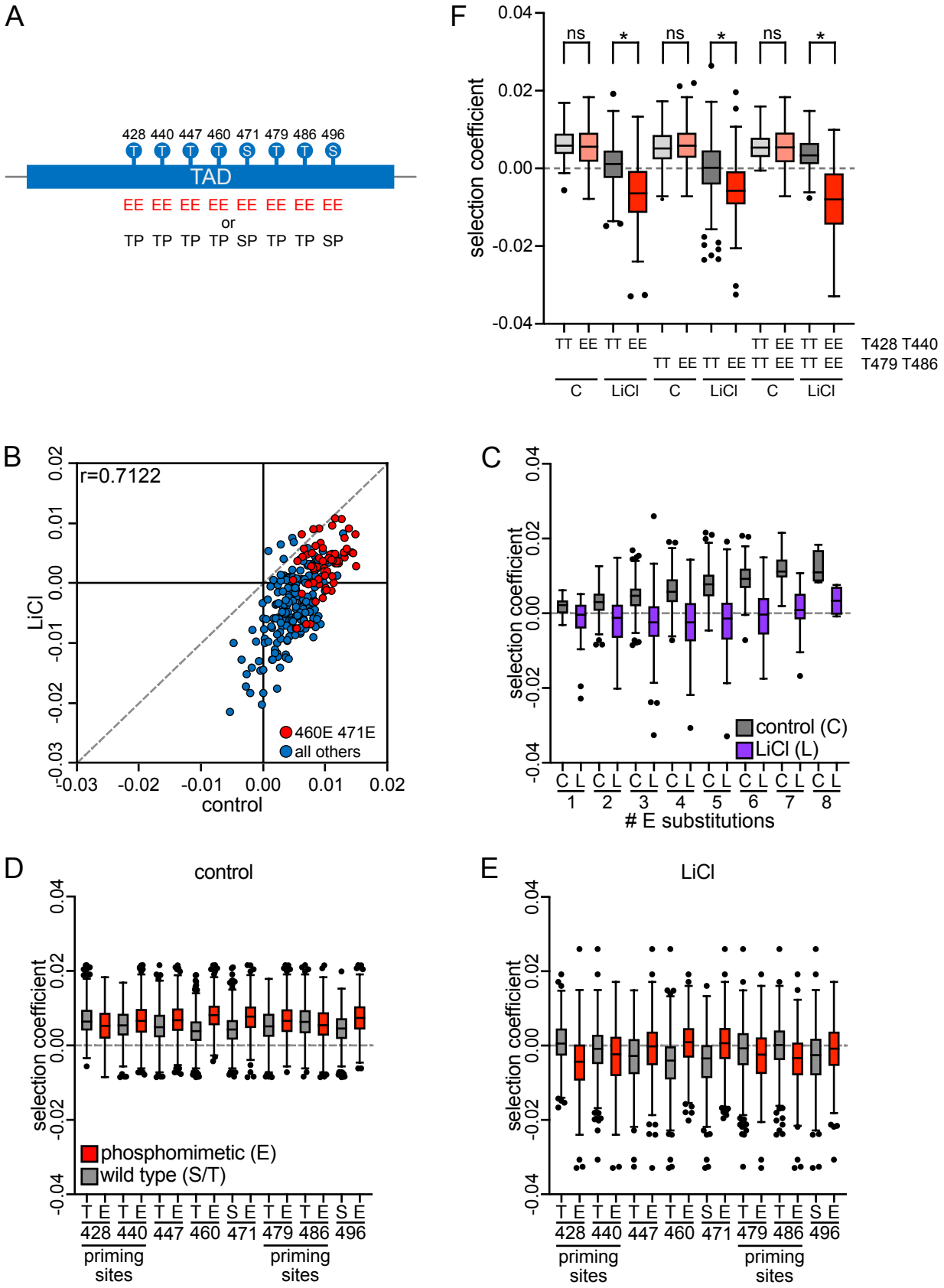
A
428 440 447 460 471 479 486 496
T T T T S T T S
TAD
EE EE EE EE EE EE EE EE
or
TP TP TP TP SP TP TP SP
F
selection coefficient
ns * ns * ns *
TT EE TT EE TT EE TT EE TT EE TT EE
T428 T440
T479 T486
C LiCl C LiCl C LiCl
B
r=0.7122
LiCl
control
460E 471E
all others
C
selection coefficient
control (C)
LiCl (L)
E substitutions
D
control
selection coefficient
phosphomimetic (E)
wild type (S/T)
priming sites
priming sites
E
LiCl
selection coefficient
priming sites
priming sites

Figure 5

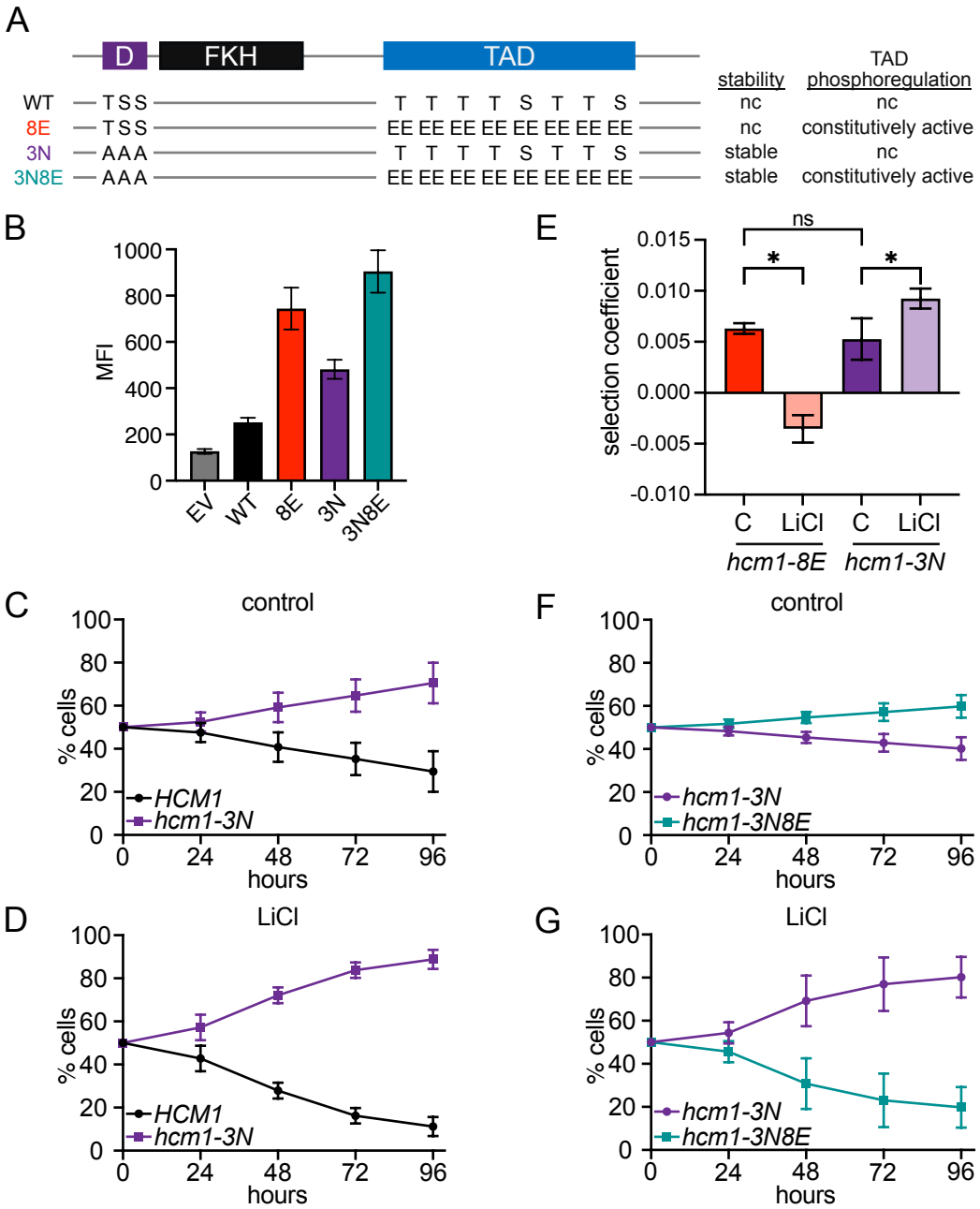
A
D
FKH
TAD
stability
TAD phosphoregulation
WT TSS T T T T S T T S nc nc
8E TSS EE EE EE EE EE EE EE EE nc constitutively active
3N AAA T T T T S T T S stable nc
3N8E AAA EE EE EE EE EE EE EE EE stable constitutively active
B
MFI
EV
WT
8E
3N
3N8E
E
selection coefficient
ns
C
LiCl
hcm1-8E
hcm1-3N
C
control
% cells
hours
HCM1
hcm1-3N
F
hcm1-3N8E
D
LiCl
G

Figure 6

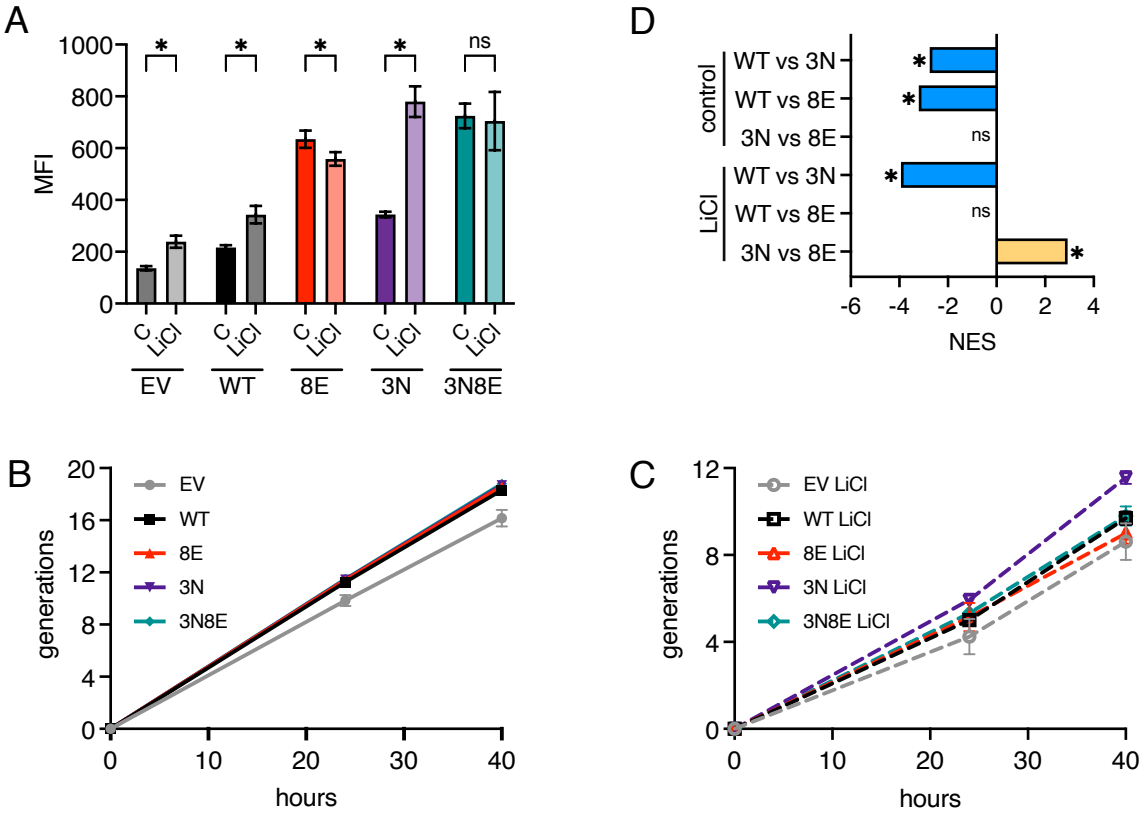
A
MFI
1000
800
600
400
200
0
*
*
*
*
ns
C
LiCl
EV
WT
8E
3N
3N8E
D
control
LiCl
WT vs 3N
WT vs 8E
3N vs 8E
ns
-6
-4
-2
0
2
4
NES
B
generations
hours
EV
WT
8E
3N
3N8E
C
EV LiCl
WT LiCl
8E LiCl
3N LiCl
3N8E LiCl